

8600 NI 3658  
NACA

# NATIONAL ADVISORY COMMITTEE FOR AERONAUTICS

TECHNICAL NOTE 3658

IMPINGEMENT OF WATER DROPLETS ON A RECTANGULAR  
HALF BODY IN A TWO-DIMENSIONAL INCOMPRESSIBLE  
FLOW FIELD

By William Lewis and Rinaldo J. Brun

Lewis Flight Propulsion Laboratory  
Cleveland, Ohio



Washington  
February 1956

IMPINGEMENT OF WATER DROPLETS ON A RECTANGULAR HALF BODY IN A TWO-  
DIMENSIONAL INCOMPRESSIBLE FLOW FIELD

By William Lewis and Rinaldo J. Brun

SUMMARY

Trajectories of water droplets moving in the ideal two-dimensional flow field ahead of a body of rectangular cross section and infinite extent in the downstream direction have been calculated by means of a differential analyzer. Data on collection efficiency and distribution of water impingement are presented.

INTRODUCTION

As part of a comprehensive research program dealing with the problem of icing protection for aircraft, an investigation of the impingement of cloud droplets on airfoils and other aircraft components has been undertaken by the NACA Lewis laboratory. In addition to specific aircraft components (refs. 1 to 3), certain general aerodynamic bodies such as cylinders (ref. 4) and ellipsoids of revolution (ref. 5) have been studied because various aircraft components may be approximately represented by these shapes. Among the general body shapes of interest is that of a rectangular body having a flat surface facing the airstream. Such a body may be used as an approximation to the shape of the sensing elements of certain instruments used to measure icing-cloud properties.

Cloud-droplet size and size distribution are sometimes measured by collecting samples of cloud droplets on small transparent slides coated with oil or some water-sensitive substance (refs. 6 to 8). The slides are then photographed to obtain a record of the droplet size distribution. Various types of sampling devices have been used in which the collecting element is usually a flat surface perpendicular to the airstream. The evaluation of the cloud-droplet size distribution from samples obtained in this way requires a knowledge of the relation between droplet diameter and collection efficiency. Droplet-impingement data applicable to a body of rectangular cross section would also be useful in estimating the collection efficiency of the central portion of the rotating-disk icing-rate meter (refs. 7 to 9) and the rectangular bars used to measure the spray distribution in an icing wind tunnel (ref. 10).

Trajectory calculations based on ideal two-dimensional flow about a ribbon (ref. 11), which is essentially a rectangle of zero chord, have been used as an approximation to obtain the impingement on rectangular bodies of finite chord. However, the ideal flow field ahead of a ribbon is not a very satisfactory representation of the actual flow field in front of a rectangular body because of the dependence of the flow ahead of the body on conditions existing behind the body.

The ideal flow field about a ribbon is symmetrical fore and aft, as shown in figure 1(a), with the streamlines closing in directly behind the body. In the case of real flow about a rectangular body, on the other hand, the streamlines cannot be calculated exactly; but general knowledge of the flow about solid boundaries suggests that the flow field is something like that shown schematically in figure 1(b). Flow separation occurs at the edge, and a wake is formed extending downstream. The effect of variations in the ratio of chord to thickness cannot be estimated accurately, but is probably small, since the wake is roughly equivalent to an indefinite downstream extension of the body.

Potential flow exists outside the limits of the boundary layer and wake (shown approximately by the dashed line). Figure 1(c) shows the ideal-flow streamlines around a rectangular half body (a body of infinite extent downstream). This flow field resembles the estimated real flow in figure 1(b) much more closely than does the ideal flow about a ribbon (fig. 1(a)). The effect of the downstream extent of the body on the flow field ahead is shown in figure 1(d), which is a superposition of portions of the fields shown in figures 1(a) and (c). The comparison shows that the presence of the afterbody exerts a considerable influence on the flow field ahead of the body.

The ideal flow field of the rectangular half body represents a closer approximation to real flow than does the ideal flow about a ribbon; however, it too is subject to the disadvantage that the velocity becomes infinite at the corner. In spite of this disadvantage, the ideal flow field in front of the rectangular half body was used, in the calculation of trajectories, because it was considered to be sufficiently realistic to yield approximate results of practical value and because the velocity components could be calculated without too much difficulty.

#### SYMBOLS

The following symbols are used in this report:

- |     |                                    |
|-----|------------------------------------|
| A   | area per unit span, sq ft/ft       |
| a   | droplet radius, ft                 |
| B,C | empirical constants, dimensionless |

$C_D$	coefficient of drag, dimensionless
$E$	collection efficiency, dimensionless
$f$	functional relation between $y_0$ and $y_s$
$G$	flux of liquid water per unit span, slugs/(sec)(ft)
$K$	inertia parameter, dimensionless
$L$	half width of rectangle, ft
$n$	impingement distribution index, dimensionless
$p, q$	arbitrary numbers
$Re$	local Reynolds number with respect to droplet, dimensionless
$Re_0$	free-stream Reynolds number with respect to droplet, dimensionless
$t$	time, sec
$U$	free-stream velocity, ft/sec
$u_x, u_y$	local air velocity components, ratio to free-stream velocity, dimensionless
$v_x, v_y$	local droplet velocity components, ratio to free-stream velocity, dimensionless
$W$	total rate of water impingement per unit span, slugs/(sec)(ft)
$W_y$	local rate of water impingement per unit area, slugs/(sec)(sq ft)
$w$	free-stream liquid-water content, slugs/cu ft
$x, y$	rectangular coordinates, ratio to half width $L$ , dimensionless
$Y$	distance from centerline ( $Y = Ly$ ), ft
$y_0$	trajectory starting ordinate, dimensionless
$y_s$	trajectory ordinate at point of impingement, dimensionless
$\beta$	local impingement efficiency, dimensionless

$\beta_0$	local impingement efficiency at centerline
$\beta_1$	local impingement efficiency at edge
$\mu$	viscosity of air, slugs/(ft)(sec)
$\rho_a$	density of air, slugs/cu ft
$\rho_w$	density of water, slugs/cu ft
$\tau$	dimensionless time function, $\tau = \frac{tU}{L}$
$\Phi$	$Re_0^2/K$ , dimensionless

#### ANALYSIS

In order to find the rate and distribution of droplet impingement on the surface of a body, it is necessary to determine the cloud-droplet trajectories with respect to the body. The method used in this case to calculate the trajectories of cloud droplets is described fully in reference 4. Assumptions that are necessary to the solution of the problem are: (1) At a large distance ahead of the body the droplets are at rest with respect to the air; (2) the only external force acting on the droplets is the drag force due to the relative velocity of the air with respect to the droplets; and (3) the droplets are always spherical and do not change in size.

#### Differential Equations of Droplet Motion

The differential equations that describe the motion of the droplets were obtained by equating the drag force with the rate of change of momentum of the droplet (ref. 4). The equations are expressed in dimensionless form in order to maintain the number of calculations at a minimum and to simplify the presentation of the results. They apply to the motion of droplets in a plane perpendicular to the edges of the rectangular half body in the system of rectangular coordinates shown in figure 2. The origin is located at the center of the front face of the rectangle, and the unit of distance is the half width  $L$  of the rectangle. The dimensionless coordinates  $x$  and  $y$  are ratios to  $L$ . The dimensionless air velocity components  $u_x$  and  $u_y$  and droplet velocity components  $v_x$  and  $v_y$  are ratios to the free-stream velocity  $U$ , which is the unit of velocity. Time is expressed in terms of the dimensionless quantity  $\tau = tU/L$ . The unit of time is the time required to go a distance  $L$  at

a speed  $U$ . At a large distance ahead of the body, a uniform air flow bearing cloud droplets is assumed to be approaching the rectangle from the negative  $x$  direction moving parallel to the  $x$  axis at a speed  $U$  (fig. 2).

The equations of motion of the droplets are

$$\left. \begin{aligned} \frac{dv_x}{d\tau} &= \frac{C_D Re}{24} \frac{1}{K} (u_x - v_x) \\ \frac{dv_y}{d\tau} &= \frac{C_D Re}{24} \frac{1}{K} (u_y - v_y) \end{aligned} \right\} \quad (1)$$

where  $Re$  is the local Reynolds number with respect to the droplet diameter  $2a$  and the local relative velocity between the air and the droplet, thus

$$Re = \frac{2a\rho_a U}{\mu} \sqrt{(u_x - v_x)^2 + (u_y - v_y)^2} \quad (2)$$

The coefficient in equation (2) is called the free-stream Reynolds number  $Re_0$ ; hence,

$$Re_0 = \frac{2a\rho_a U}{\mu} \quad (3)$$

The dimensionless number,  $K$ , the inertia parameter, is defined as follows:

$$K = \frac{2}{9} \frac{\rho_w a^2 U}{\mu L} \quad (4)$$

The coefficient of drag  $C_D$  may be obtained from experimental data as a function of the local droplet Reynolds number  $Re$ .

An examination of equations (1) and (2) shows that the characteristics of the trajectories depend only on the values of the two dimensionless parameters  $K$  and  $Re_0$ . Thus, a unique set of droplet trajectories exists for every combination of  $K$  and  $Re_0$ .

#### Method of Solution

The differential equations of motion (1) are difficult to solve because values of the velocity components and the factor containing the

coefficient of drag depend on the position and velocity of the droplet at each instant and, therefore, are not known until the trajectory is traced. The values of these quantities must be fed into the equations as a trajectory is developed. This was accomplished by using a mechanical differential analyzer constructed at the NACA Lewis laboratory for this purpose (ref. 4). The results were obtained in the form of plots of droplet trajectories in the coordinates of figure 2.

The following information was required for use with the differential analyzer in the trajectory calculation:

(1) Coefficient of drag data: Values of the factor  $C_D Re/24$  as a function of  $Re$  were obtained from tables in reference 11.

(2) Air velocity components: The air velocity components  $u_x$  and  $u_y$  were determined as functions of  $x$  and  $y$  by means of an analytical solution of the two-dimensional potential flow field ahead of a rectangular half body. Because of symmetry with respect to the centerline (see fig. 1), one half of this field is identical to the flow field around a step discontinuity in the floor of a channel of infinite depth, a configuration discussed in reference 12. The equations used to calculate the velocity components were obtained by means of the Schwarz-Christoffel transformation as described in reference 12. These equations, expressed in parametric form, are as follows:

$$\left. \begin{aligned} u_x &= \frac{\sinh p \cosh p - \sinh p \cos q}{\sin^2 q + \sinh^2 p} \\ u_y &= \frac{\cosh p \sin q - \sin q \cos q}{\sin^2 q + \sinh^2 p} \\ x &= \frac{-1}{\pi} (p + \sinh p \cos q) \\ y &= \frac{1}{\pi} (q + \cosh p \sin q) \end{aligned} \right\} \quad (5)$$

Any pair of values of the arbitrary parameters  $p$  and  $q$  determines the coordinates  $x$  and  $y$  of a point in the flow field and the components  $u_x$  and  $u_y$  of the velocity at that point. Values of  $u_x$ ,  $u_y$ ,  $x$ , and  $y$  were calculated from equation (5) for a number of points in the flow field ahead of the rectangle, and curves giving  $u_x$  and  $u_y$  as functions of  $x$  and  $y$  were obtained by cross-plotting. The calculated values of coordinates and air velocity components are presented in table I.

(3) Starting conditions: The integrations were started at  $x = -60$  where the air velocity components are  $u_x = 0.9945$  and  $u_y = 0.0001y$  for all values of  $y$  between 0 and 1. The initial droplet velocity components were assumed to be  $v_x = 0.9945$  and  $v_y = 0$ . The calculations were performed in three steps:  $x = -60$  to  $-10$ ;  $x = -10$  to  $-1$ ; and  $x = -1$  to 0. Different scale factors were used on the machine for each step, and the results of each of the first two steps were used to establish starting conditions for the succeeding step.

#### Determination of Droplet Impingement

The differential analyzer traces the trajectories of the droplets from a starting point defined by the ordinate  $y_0$  at a large distance ahead of the body to the final point of impingement having the ordinate  $y_s$  at the surface of the rectangle. The trajectories provide pairs of values of  $y_0$  and  $y_s$  that establish the relation between  $y_0$  and  $y_s$  for various combinations of  $K$  and  $Re_0$ . The relation is expressed symbolically as follows:

$$y_0 = f(y_s) \quad (6)$$

and the symbols  $f(0)$  and  $f(1)$  are used to denote the values assumed by  $y_0$  when  $y_s$  is 0 and 1, respectively.

If a rectangular body of half width  $L$  moves through a cloud of uniform liquid-water content and uniform droplet size, the flux of liquid water per unit span between any two trajectories with starting ordinates  $Ly_{0,1}$  and  $Ly_{0,2}$  ( $Ly_0$  has the dimensions of length) is

$$G = UwL(y_{0,2} - y_{0,1})$$

Since the trajectories define the path of the flow of liquid water, the same flux arrives at the rectangle surface between the trajectory terminal ordinates  $Ly_{s,1}$  and  $Ly_{s,2}$  corresponding to the starting ordinates  $Ly_{0,1}$  and  $Ly_{0,2}$ . The surface area per unit span of the strip of the rectangle between the two terminal ordinates  $Ly_{s,1}$  and  $Ly_{s,2}$  is

$$A = L(y_{s,2} - y_{s,1})$$

The liquid-water flux  $G$  is distributed over the area  $A$ ; hence, the average rate of water impingement per unit area on this strip is

$$\frac{G}{A} = \frac{UwL(y_{0,2} - y_{0,1})}{L(y_{s,2} - y_{s,1})}$$

If  $y_{s,1}$  is allowed to approach  $y_{s,2}$  as a limit, the limit approached by  $G/A$  is the local rate of water impingement  $W_y$  at the distance  $Y = y_s L$  from the centerline.

$$W_y = \lim_{A \rightarrow 0} \frac{G}{A} = Uw \frac{dy_0}{dy_s} \quad (7)$$

The local impingement efficiency  $\beta$  is defined as follows:

$$\beta = \frac{W_y}{Uw} \quad (8)$$

Hence,

$$\beta = \frac{dy_0}{dy_s} \quad (9)$$

The total rate of water interception per unit span over the entire face of the rectangle is twice the integral of the local impingement rate from the stagnation point ( $Y = 0$ ) to the outside edge ( $Y = L$ ); thus,

$$W = 2 \int_0^L Uw\beta dY = 2LUw \int_0^1 \frac{dy_0}{dy_s} dy_s$$

$$W = 2LUw[f(1) - f(0)]$$

where the symbol  $f$  refers to the function of equation (6).

In a symmetrical flow field, a droplet approaching the stagnation point along the central streamline does not change direction; thus, the value of  $y_0$  corresponding to  $y_s = 0$  is 0; therefore,

$$W = 2LUwf(1) \quad (10)$$

The collection efficiency  $E$  is defined as follows:

$$E = \frac{W}{2LUw} \quad (11)$$

Hence,

$$E = f(1) \quad (12)$$

The collection efficiency is therefore equal to the value of  $y_0$  when  $y_s = 1$ , which is the nondimensional starting ordinate of the trajectory that strikes the outside edge of the rectangle in the coordinate system of figure 2.

### RESULTS

A total of 74 pairs of values of  $y_0$  and  $y_s$  were calculated with the differential analyzer using 23 combinations of  $Re_0$  and  $K$ . It was found that the relation of equation (6) between  $y_0$  and  $y_s$  for any particular combination of  $K$  and  $Re_0$  could be represented approximately by an empirical equation of the form

$$y_0 = By_s + Cy_s^n \quad (13)$$

where  $B$  and  $C$  are positive and less than 1 and  $n$  is positive and greater than 1. The collection efficiency  $E$  is the value of  $y_0$  when  $y_s = 1$ ; hence,

$$E = B + C \quad (14)$$

The local impingement efficiency  $\beta$  may be obtained by differentiating equation (13) as follows:

$$\beta = \frac{dy_0}{dy_s} = B + nCy_s^{(n-1)} \quad (15)$$

The local impingement efficiency at the stagnation point  $\beta_0$  is obtained by setting  $y_s = 0$  in equation (15); thus,

$$B = \beta_0$$

and from equation (14),

$$C = E - \beta_0$$

Substituting in equation (13) gives

$$y_0 = \beta_0 y_s + (E - \beta_0) y_s^n \quad (16)$$

and from equation (15) there is obtained

$$\beta = \beta_0 + n(E - \beta_0)y_s^{(n-1)} \quad (17)$$

Equation (17) shows that the local impingement efficiency has a minimum value  $\beta_0$  at the stagnation point and increases to a maximum given by

$$\beta_1 = \beta_0 + n(E - \beta_0) \quad (18)$$

at the outside edges of the rectangle.

The impingement pattern corresponding to any given pair of values of  $K$  and  $Re_0$  is determined by three parameters: (1) the collection efficiency  $E$ , (2) the local impingement efficiency at the stagnation point  $\beta_0$ , and (3) the distribution index  $n$ , which determines the form of the distribution of impingement.

An analysis of the trajectory data has shown that these three parameters, which are functions of  $K$  and  $Re_0$ , may be represented approximately by the following empirical equations:

$$n = 1 + e^{-\frac{1}{K}} + \frac{400}{Re_0 + 32} [1.1 + (\log_e 0.72 K)^2]^{-2} \quad (19)$$

$$-\log_e \beta_0 = \left( \frac{11}{K + 10} + 0.2 + 0.0238 Re_0^{0.538} \right) \left( 1.16 - \frac{87}{115 + Re_0 + 0.004 Re_0^2} \right) (K - 0.28)^{-0.6} \quad (20)$$

$$-\log_e E = \left( \frac{151}{K^2 + 150} + 0.267 + 0.225 Re_0^{0.28} \right) \left( 1.02 - \frac{180}{250 + Re_0} \right) (K - 0.15)^{-0.74} \quad (21)$$

Equations (17), (19), (20), and (21) provide a means of determining approximately the collection efficiency and the distribution of impingement for any combination of  $Re_0$  and  $K$ . The trajectory calculations used in deriving the equations adequately covered a range of  $K$  from  $1/2$  to 10 and of  $Re_0$  from 16 to 256. Outside this range the equations represent extrapolations.

Values of  $n$ ,  $\beta_0$ , and  $E$  calculated from the empirical equations are presented in figures 3, 4, and 5, respectively. The 74 values of  $y_0$  obtained with the differential analyzer and the corresponding values calculated from the equations are presented for comparison in table II. The standard deviation of the differences between corresponding values is 0.0051; therefore, the probable error involved in using the equations to determine  $y_0$  is  $\pm 0.0034$  based on the assumption that the results from the trajectories are absolutely correct. The dimensionless parameters  $Re_0$  and  $K$  are defined in equations (3) and (4). Equations and graphs for use in determining values of  $K$  and  $Re_0$  in terms of air speed, altitude, body size, and droplet diameter in practical units are presented in reference 13.

### DISCUSSION

The use of empirical equations to represent the impingement patterns is essentially a means of interpolating and extrapolating the trajectory data. The procedure is analogous to that of drawing a family of curves and interpolating between them. Because of random errors in the trajectory data, a certain amount of smoothing is necessary in using either procedure. The use of empirical equations has the advantage of accomplishing the smoothing operation in a consistent manner over the entire range of  $K$  and  $Re_0$ , thus assuring that the results are as accurate for intermediate values of these parameters as for the values for which trajectories were calculated. The equations also provide a more reliable basis for extrapolation to values of  $K$  and  $Re_0$  beyond the range of the trajectory calculations.

The average accuracy of the equations is probably a little better than is indicated by the probable error of  $\pm 0.0034$  in  $y_0$  based on the departures in table II, because these deviations are due partly to errors in the trajectory calculations. The same degree of accuracy (probable error about 0.003) also applies to values of  $E$  and  $\beta_0$  from equations (20) and (21). Values of  $\beta$  at intermediate points and values of  $\beta_1$  at the corner of the rectangle, calculated from equations (17) and (18), may be subject to larger errors because of the effect of errors in the distribution index  $n$ .

The validity of the representation of the impingement distribution patterns given by equation (17), using values of  $n$ ,  $\beta_0$ , and  $E$  from equations (19), (20), and (21), respectively, can be checked by a comparison with average values of  $\beta$  for the intervals of  $y_s$  between adjacent trajectories. Such values are obtained directly from the trajectory data by means of the relation

$$\bar{\beta} = \frac{\Delta y_0}{\Delta y_s} \quad (22)$$

The comparison is shown in figure 6 in which the smooth curves were calculated from equation (17), and the block diagrams represent averages from equation (22) based on individual intervals between adjacent calculated trajectories. An examination of figure 6 reveals the general pattern of the impingement distribution as a function of  $K$  and  $Re_0$ .

At high values of  $K$ , the impingement efficiency approaches 1 across the entire face of the rectangle, but more slowly for high values of  $Re_0$ .

At low values of  $K$ , the impingement efficiency approaches 0, but the number of trajectories calculated (3 at  $K = 1/3$ ) is too small to determine accurately the shape of the impingement profile. For all values of  $K$ , the impingement efficiency decreases, and the distribution becomes more uniform with increasing  $Re_0$ . The greatest curvature of the impingement profile, indicating a sharp maximum impingement at the edge, occurs at low values of  $Re_0$  and values of  $K$  between 1 and 2. The curves calculated from equation (17) agree satisfactorily with the values of  $\bar{\beta}$  obtained from adjacent trajectories over the entire range of  $K$  and  $Re_0$  for which trajectories were determined. Equation (17), therefore, provides a consistent representation of the variations of the impingement profile with  $K$  and  $Re_0$ .

It is of interest to compare the droplet-impingement data for a rectangle with similar data for a ribbon in reference 11. The results are presented in reference 11 in the form of curves showing  $E$  and  $\beta_0$  as functions of  $K$  and  $\phi$  ( $\phi = Re_0^2/K$ ). Values of  $E$  and  $\beta_0$  read from these curves are compared in table III with values calculated from equations (16) and (17) for corresponding values of  $K$  and  $Re_0$ . For most values of  $K$  and  $\phi$  the rectangle has a lower collection efficiency than the ribbon; this effect is due to the influence of the afterbody in reducing the rate of deceleration of the air in the region just ahead of the body.

It was pointed out in the discussion of flow fields in the INTRODUCTION that the flow field of the rectangular half body differs from that of the ribbon by the addition of an afterbody, but that both differ from the real flow about a rectangular body because of the absence of flow separation and because of the requirement of infinite velocity at the edges. An examination of the comparative streamlines in figure 1(d) shows a great difference in velocity in the immediate vicinity of the edge. (Velocity is inversely proportional to streamline spacing.) In spite of the difference in the flow fields, however, the differences in collection efficiency of the ribbon and rectangle are only moderate. The maximum

difference in table III is 0.099 at  $K = 2$  and  $\phi = 10,000$ , and the average difference for all values in table III is 0.026. These facts suggest that the results obtained using the ideal flow ahead of the rectangular half body are likely to be a fairly good approximation to the actual impingement on a rectangular body in real flow. The largest difference between the ideal flow and the real flow is that the ideal flow permits a high local air velocity in the neighborhood of the edge; however, these differences in local air velocity in the neighborhood of the edge have a relatively small effect on the trajectories.

#### CONCLUDING REMARKS

The rate and distribution of water impingement on a semi-infinite rectangular body moving in a cloud of uniform liquid-water content and droplet size have been determined by means of droplet trajectory calculations. Empirical equations have been found providing an approximate representation of the impingement rate and distribution in terms of the inertia parameter  $K$  and the free-stream droplet Reynolds number  $Re_0$ . Equation (17) gives the local impingement efficiency  $\beta$  as a function of distance from the centerline of the rectangle in terms of the following three parameters: (1) the collection efficiency  $E$ , (2) the impingement efficiency at the centerline  $\beta_0$ , and (3) the impingement distribution index  $n$ .

These parameters may be determined from  $K$  and  $Re_0$  by means of empirical equations (19), (20), and (21).

Lewis Flight Propulsion Laboratory  
National Advisory Committee for Aeronautics  
Cleveland, Ohio, December 14, 1955

#### REFERENCES

1. Brun, Rinaldo J., Gallagher, Helen M., and Vogt, Dorothea E.: Impingement of Water Droplets on NACA 65A004 Airfoil and Effect of Change in Airfoil Thickness from 12 to 4 Percent at  $4^\circ$  Angle of Attack. NACA TN 3047, 1953.
2. Dorsch, Robert G., and Brun, Rinaldo J.: A Method for Determining Cloud-Droplet Impingement on Swept Wings. NACA TN 2931, 1953.
3. Hacker, Paul T., Brun, Rinaldo J., and Boyd, Bemrose: Impingement of Droplets in  $90^\circ$  Elbows with Potential Flow. NACA TN 2999, 1953.

4. Brun, Rinaldo J., and Mergler, Harry W.: Impingement of Water Droplets on a Cylinder in an Incompressible Flow Field and Evaluation of Rotating Multicylinder Method for Measurement of Droplet-Size Distribution, Volume-Median Droplet Size, and Liquid-Water Content in Clouds. NACA TN 2904, 1953.
5. Dorsch, Robert G., Brun, Rinaldo J., and Gregg, John L.: Impingement of Water Droplets on an Ellipsoid with Fineness Ratio 5 in Axisymmetric Flow. NACA TN 3099, 1954.
6. Bigg, F. J., and Abel, G. C.: Note on Sampling and Photographing Cloud Droplets in Flight. Tech. Note Mech. Eng. 156, British R.A.E., Sept. 1953.
7. Pettit, K. G.: Nephelometric Instrumentation for Aircraft Icing Research. Rep. No. MD-33, Nat. Res. Council of Canada (Ottawa), Aug. 1950.
8. Vonnegut, B., Cunningham, R. M., and Katz, R. E.: Instruments for Measuring Atmospheric Factors Related to Ice Formation on Airplanes. De-Icing Res. Lab., Dept. Meteorology, M.I.T., Apr. 1946.
9. Lewis, William, and Hoecker, Walter H., Jr.: Observations of Icing Conditions Encountered in Flight During 1948. NACA TN 1904, 1949.
10. von Glahn, Uwe H., Gelder, Thomas F., and Smyers, William H., Jr.: A Dye-Traces Technique for Experimentally Obtaining Impingement Characteristics of Arbitrary Bodies and a Method for Determining Droplet Size Distribution. NACA TN 3338, 1955.
11. Langmuir, Irving, and Blodgett, Katherine B.: A Mathematical Investigation of Water Droplet Trajectories. Tech. Rep. No. 5418, Air Materiel Command, AAF, Feb. 19, 1946. (Contract No. W-33-038-ac-9151 with General Electric Co.)
12. Milne-Thomson, Louis Melville: Theoretical Aerodynamics. New York, D. Van Nostrand Co., 1948.
13. Brun, Rinaldo J., Gallagher, Helen M., and Vogt, Dorothea E.: Impingement of Water Droplets on NACA 65<sub>1</sub>-208 and 65<sub>1</sub>-212 Airfoils at 4° Angle of Attack. NACA TN 2952, 1953.

TABLE I. - VELOCITY FIELD AHEAD OF RECTANGULAR HALF BODY

[The table gives values of the dimensionless space coordinates  $x$  and  $y$  and corresponding values of dimensionless velocity components  $u_x$  and  $u_y$  (see fig. 2) calculated from equation (5).]

$x$	$y$	$u_x$	$u_y$	$x$	$y$	$u_x$	$u_y$
-0.09567	0	0.07485	0	0	0.12551	0	0.09918
-.19242		.14889		-.09473	.12622	.07571	.09855
-.29136		.22128		-.19053	.12835	.15036	.09699
-.39364		.29132		-.28847	.13195	.22335	.09429
-.50049		.35837		-.38969	.13712	.29394	.09073
-.61323		.42191		-.49538	.14395	.3615	.08637
-.73335		.48154		-.60686	.15260	.4253	.08142
-.86246		.53707		-.72556	.16328	.4852	.07603
-1.0518		.60437		-.85310	.17622	.5408	.07040
-1.2655		.66404		-1.0400	.19750	.6081	.06275
-1.6451		.73977		-1.2507	.22419	.6677	.05523
-2.1190		.80050		-1.6248	.27674	.7432	.04469
-2.9586		.86173		-2.0914	.34869	.8033	.03542
-4.1437		.90515		-2.9171	.48638	.8639	.02536
-6.3798		.94138		-4.0816	.69271	.9067	.01779
-9.9599		.96403		-6.2771	1.0996	.9424	.01119
-11.96		.97045		-9.7905	1.7711	.9647	.00695
-14.40		.97580		0	.24681	0	.19892
-17.30		.98010		-.09202	.24818	.07782	.19774
-20.9		.98368		-.18505	.25233	.15466	.19434
-25.2		.98660		-.28009	.25935	.22960	.18880
-30.5		.98903		-.37821	.26940	.30184	.18144
-37.0		.99100		-.48056	.28271	.3707	.17251
-44.8		.99264		-.58836	.29957	.4356	.16237
-54.5		.99397		-.70299	.32036	.4960	.15138
-66.0		.99505		-.82589	.34556	.55204	.13995
-98		.99668		-1.00567	.38700	.61937	.12446
-145		.99777		-1.2079	.43897	.67846	.10929
-216		.99851		-1.5659	.54132	.75277	.08814
-320		.99900		-2.0110	.68141	.81161	.06968

TABLE I. - Continued. VELOCITY FIELD AHEAD OF RECTANGULAR HALF BODY

[The table gives values of the dimensionless space coordinates  $x$  and  $y$  and corresponding values of dimensionless velocity components  $u_x$  and  $u_y$  (see fig. 2) calculated from equation (5).]

$x$	$y$	$u_x$	$u_y$	$x$	$y$	$u_x$	$u_y$
-2.7964	0.94955	0.87027	0.04975	-0.14923	0.58990	0.19037	0.52027
-3.9010	1.3514	.91143	.03482	-.22535	.60516	.25295	-----
0	.36350	0	.30257	-.30333	.62702	.36594	.47837
-.08763	.36549	.08318	.30063	-.38384	.65597	.44476	.45015
-.17617	.37150	.16220	.29528	-.46762	.69261	.51652	.41876
-.26652	.38167	.24046	.28647	-.55549	.73784	.58097	.38561
-.35965	.39623	.31554	.27476	-.64834	.79265	.63827	.35190
-.45658	.41550	.38666	.26064	-.78167	.88280	.70392	.30766
-.55842	.43993	.45316	.24473	-.92848	.99580	.75851	.26574
-.66641	.47005	.51469	.22756	0	.66908	0	.66820
-.78186	.50656	.57037	.20947	-.06609	.67239	.10801	.66394
-.95012	.56659	.63835	.18583	-.13259	.68241	.21326	.64699
-1.1386	.64187	.69669	.16258	-.19992	.69936	.31323	.62186
-1.4706	.79014	.76902	.13044	-.26854	.72361	.40600	.58914
-1.8804	.99310	.82538	.10266	-.33890	.75573	.49028	.55077
-2.6012	1.3815	.88073	.07293	-.41152	.79644	.56537	.50883
0	.47508	0	.41422	-.48696	.84664	.63121	.46506
-.08163	.47762	.08763	.41151	-.56585	.90750	.68822	.42123
-.16403	.48529	.17377	.40350	-.67760	1.0075	.75165	.36466
-.24798	.49826	.25708	.39066	0	.74914	0	.81949
-.33428	.51683	.33641	.37364	-.05716	.75266	.12466	.81181
-.42382	.54141	.41084	.35325	-.11454	.76331	.24522	.78960
-.51753	.57258	.47965	.33043	-.17235	.78129	.35810	.75456
-.61646	.61100	.54257	.30599	-.23081	.80704	.46069	.70953
-.70243	.65756	.59954	.28086	-.29017	.84113	.55148	.65756
-.87424	.73412	.66631	.24740	-.35069	.88433	.62994	.60170
-1.0440	.83015	.72327	.21528	-.41266	.93758	.69645	.54458
-1.3404	1.0193	.79232	.17142	-.47639	1.0022	.75206	.48848
0	.57788	0	.53542	0	.81831	0	1.0000
-.07431	.58087	.09618	.53158	-.04775	.82190	.14888	.98885

TABLE I. - Concluded. VELOCITY FIELD AHEAD OF RECTANGULAR HALF BODY

[The table gives values of the dimensionless space coordinates  $x$  and  $y$  and corresponding values of dimensionless velocity components  $u_x$  and  $u_y$  (see fig. 2) calculated from equation (5).]

x	y	$u_x$	$u_y$	x	y	$u_x$	$u_y$
-0.09549	0.83274	0.29131	0.95663	-0.02118	0.95495	0.32951	1.8215
-.14324	.85109	.42190	.90665	-.04176	.96398	.62023	1.6952
-.19099	.87735	.53705	.84356	-.06113	.97924	.76417	1.3668
-.23873	.91212	.63516	.77240	-.07864	1.0011	1.0088	1.3188
-.28648	.95617	.71632	.69781	0	.97508	0	2.4142
-.33423	1.0105	.78179	.62349	-.01386	.97762	.49501	2.3248
0	.87506	0	1.2203	-.02696	.98529	.90034	2.0906
-.03833	.87858	.18480	1.2034	-.03850	.99826	1.1755	1.7863
-.07645	.88923	.35876	1.1552	0	.98942	0	3.3050
-.11413	.90721	.51336	1.0817	-.00786	.99141	.85669	3.1543
-.15116	.93296	.64377	.99151	-.01482	.99742	1.4292	2.6018
-.18729	.96705	.74884	.89289	0	.99681	0	5.0275
-.22227	1.0103	.83013	.79296	-.00347	.99818	1.7229	4.3791
0	.91908	0	1.4966	0	.99959	0	10.078
-.02940	.92239	.23954	1.4687	-.00076	1.0003	4.8931	6.3865
-.05840	.93241	.45956	1.3943				
-.08656	.94936	.64606	1.2826				
-.11343	.97361	.79306	1.1508				
-.13856	1.0057	.90171	1.0130				
0	.95196	0	1.8675				

TABLE II. - COMPARISON OF CALCULATED STARTING ORDINATES

[Starting ordinates  $y_0$  of trajectories calculated with differential analyzer and corresponding values of  $y_0$  calculated from empirical equations for same values of  $y_s$  are compared.]

$Re_0$	K	$y_s$	$y_0$ (Trajectory)	$y_0$ (Equations)	Difference
0	0.5	0.676	0.228	0.227	-0.001
		1.028	.461	.461	0
16	0.333	0.507	0.033	0.037	+0.004
		.736	.062	.070	+0.008
	0.5	0.372	0.075	0.074	-0.001
		.666	.149	.149	0
		.892	.224	.225	+0.001
		.972	.265	.257	-.008
	1	0.182	0.082	0.082	0
		.367	.163	.166	+0.003
		.552	.245	.250	+0.005
		.715	.327	.327	0
		.856	.408	.405	-.003
		.986	.492	.495	+0.003
	.996	.505	.503	-.002	
	2	0.414	0.259	0.266	+0.007
.551		.346	.355	+0.009	
.807		.523	.528	+0.005	
1.012		.702	.697	-.005	
4	0.238	0.186	0.186	0	
	.472	.369	.371	+0.002	
	.703	.557	.557	0	
	.926	.740	.745	+0.005	
10	0.425	0.384	0.384	0	
	.999	.916	.916	0	
64	0.333	0.414	0.013	0.012	-0.001
		0.5	0.037	0.037	0
	.554	.054	.062	+0.008	
	.755	.088	.095	+0.007	
.904	.109	.124	+0.015		

TABLE II. - Continued. COMPARISON OF CALCULATED STARTING ORDINATES

[Starting ordinates  $y_0$  of trajectories calculated with differential analyzer and corresponding values of  $y_0$  calculated from empirical equations for same values of  $y_s$  are compared.]

$Re_0$	K	$y_s$	$y_0$ (Trajectory)	$y_0$ (Equations)	Difference	
64	1	0.127	0.040	0.037	-0.003	
		.490	.158	.146	-.012	
		.722	.237	.229	-.008	
		.974	.359	.352	-.007	
		1.035	.400	.390	-.010	
	2	0.500	0.251	0.254	+0.003	
		.644	.338	.333	-.005	
		.920	.511	.511	0	
	4	0.261	0.180	0.178	-0.002	
		.519	.361	.361	0	
		.765	.542	.545	+0.003	
		.985	.727	.720	-.007	
	10	0.443	0.378	0.378	0	
		.977	.857	.856	-.001	
	128	0.5	0.545	0.035	0.034	-0.001
			.820	.053	.060	+0.007
1		0.184	0.038	0.037	-0.001	
		.351	.077	.072	-.005	
		.515	.114	.110	-.004	
		.638	.153	.143	-.010	
		.910	.232	.233	+0.001	
2		0.399	0.164	0.164	0	
		.576	.248	.244	-.004	
		.748	.331	.331	0	
		.931	.440	.436	-.004	
4		0.287	0.176	0.174	-0.002	
		.565	.352	.354	+0.002	
		.700	.440	.446	+0.006	
		.944	.621	.621	0	

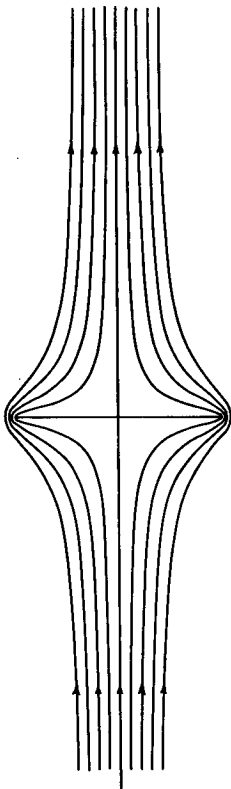
TABLE II. - Concluded. COMPARISON OF CALCULATED STARTING ORDINATES

[Starting ordinates  $y_0$  of trajectories calculated with differential analyzer and corresponding values of  $y_0$  calculated from empirical equations for same values of  $y_s$  are compared.]

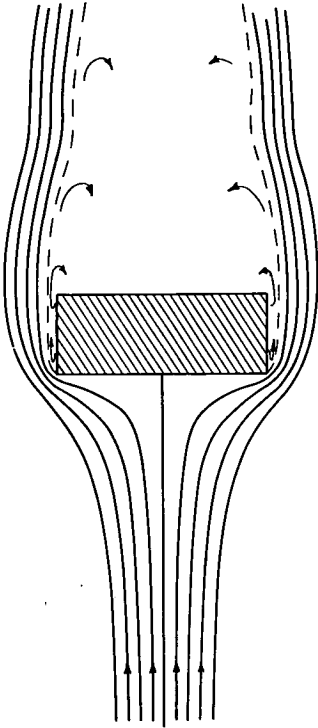
$Re_0$	K	$y_s$	$y_0$ (Trajectory)	$y_0$ (Equations)	Difference
128	10	0.461	0.372	0.373	+0.001
		.903	.751	.753	+0.002
256	0.5	0.832	0.033	0.027	-0.006
	1	0.266	0.035	0.036	+0.001
		.517	.072	.075	+0.003
		.730	.110	.115	+0.005
		.943	.148	.161	+0.013
	2	0.483	0.159	0.160	+0.001
.697		.243	.243	0	
.975		.367	.366	-.001	
4	0.466	0.259	0.251	-0.008	
	.634	.343	.349	+0.006	
	.905	.520	.516	-.004	
10	0.488	0.369	0.370	+0.001	
	.947	.746	.745	-.001	

TABLE III. - COMPARISON OF COLLECTION EFFICIENCY E AND STAGNATION-LINE IMPINGEMENT EFFICIENCY  $\beta_o$  FOR RECTANGLE AND CORRESPONDING DATA FOR RIBBON FROM REFERENCE 11 (LANGMUIR)

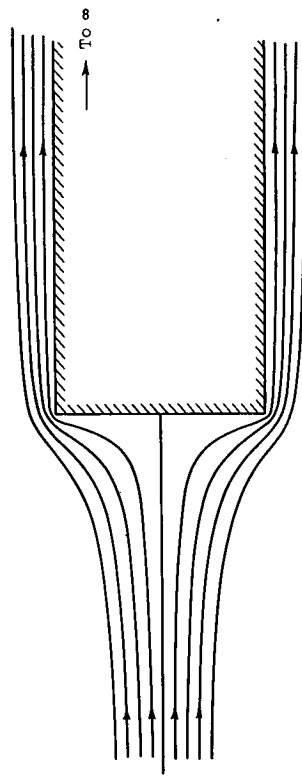
K	$\phi$ $\left(\frac{Re_o^2}{K}\right)$	E (Rectangle)	E (Ribbon)	$\beta_o$ (Rectangle)	$\beta_o$ (Ribbon)
0.25	0	0.123	0.122	0	0
	100	.060	.084		0
	1,000	.036	.062	0	0
	10,000	.011	.035	0	0
0.333	0	0.262	0.244	0.052	0.098
	100	.161	.168	.034	.076
	1,000	.113	.125	.017	.063
	10,000	.049	.075	.003	.046
0.50	0	0.436	0.450	0.287	0.235
	100	.316	.350	.231	.186
	1,000	.244	.260	.161	.154
	10,000	.134	.157	.066	.114
1	0	0.651	0.666	0.554	0.470
	100	.535	.595	.484	.380
	1,000	.452	.503	.384	.320
	10,000	.305	.382	.228	.244
2	0	0.789	0.808	0.722	0.667
	100	.691	.734	.650	.574
	1,000	.610	.666	.548	.492
	10,000	.466	.565	.388	.389
4	0	0.878	0.894	0.835	0.800
	100	.802	.836	.769	.731
	1,000	.733	.783	.676	.660
	10,000	.610	.692	.539	.544
10	0	0.953	0.954	0.928	0.909
	100	.903	.918	.874	.864
	1,000	.855	.883	.805	.823
	10,000	.773	.819	.709	.737
20	0	0.982	0.976	0.962	0.951
	100	.948	.954	.923	.921
	1,000	.915	.929	.872	.890
	10,000	.862	.882	.803	.834
100	0	0.997	0.995	0.992	0.989
	100	.982	.988	.970	.978
	1,000	.968	.980	.946	.965
	10,000	.948	.960	.912	.942



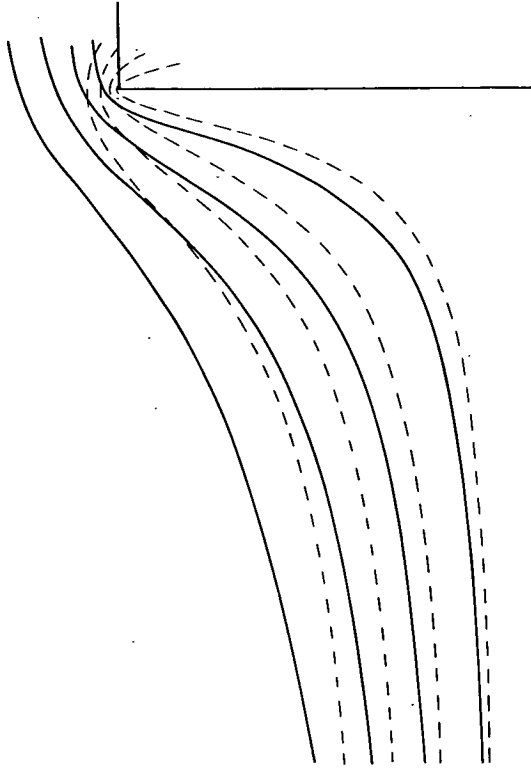
(a) Ideal flow about a ribbon.



(b) Estimated flow about a rectangle.



(c) Ideal flow about a rectangular half body.



(d) Comparison of ideal flow about ribbon and rectangular half body.

Figure 1. - Comparison of two-dimensional flow fields.

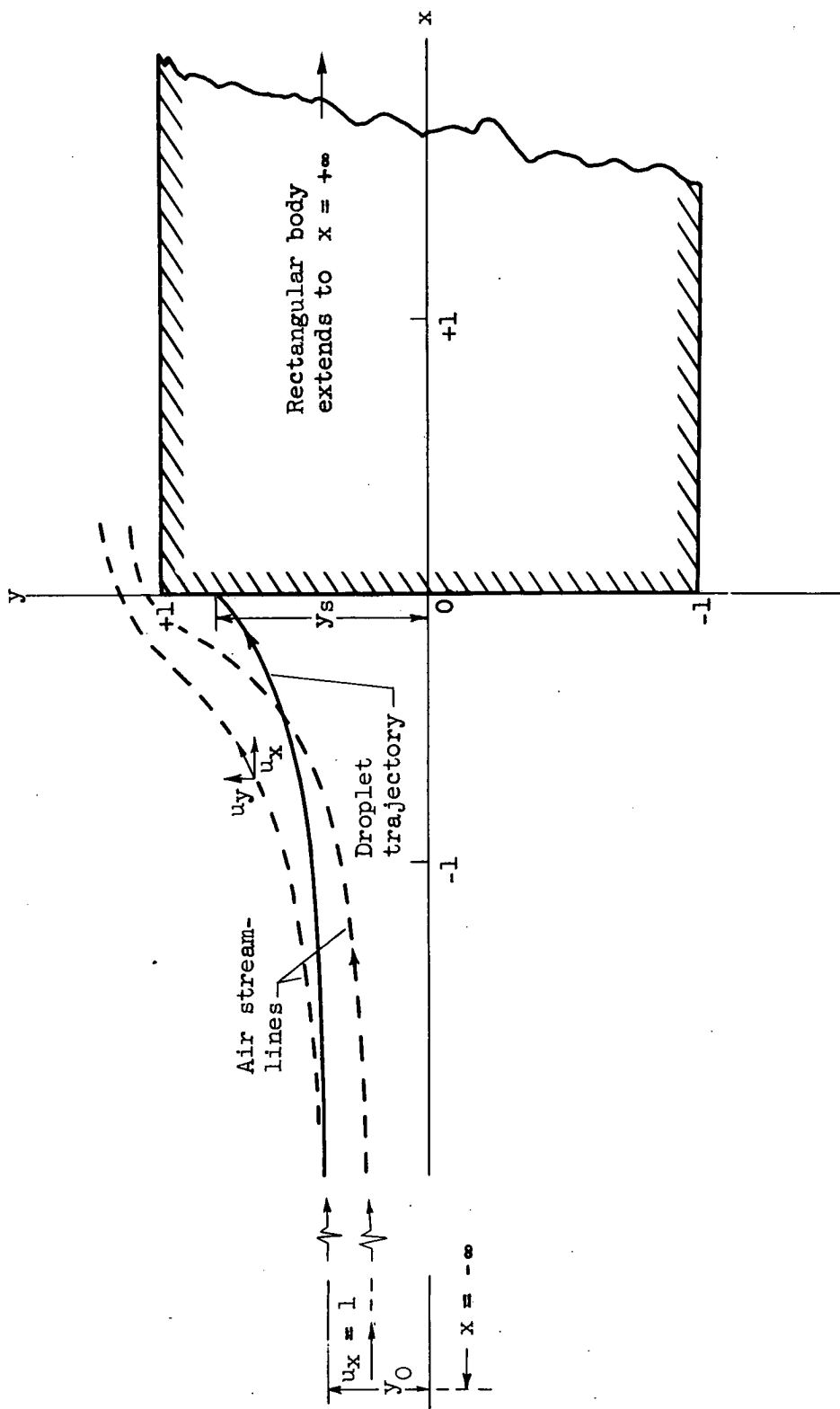


Figure 2. - Coordinate system and notation for droplet trajectory calculations.

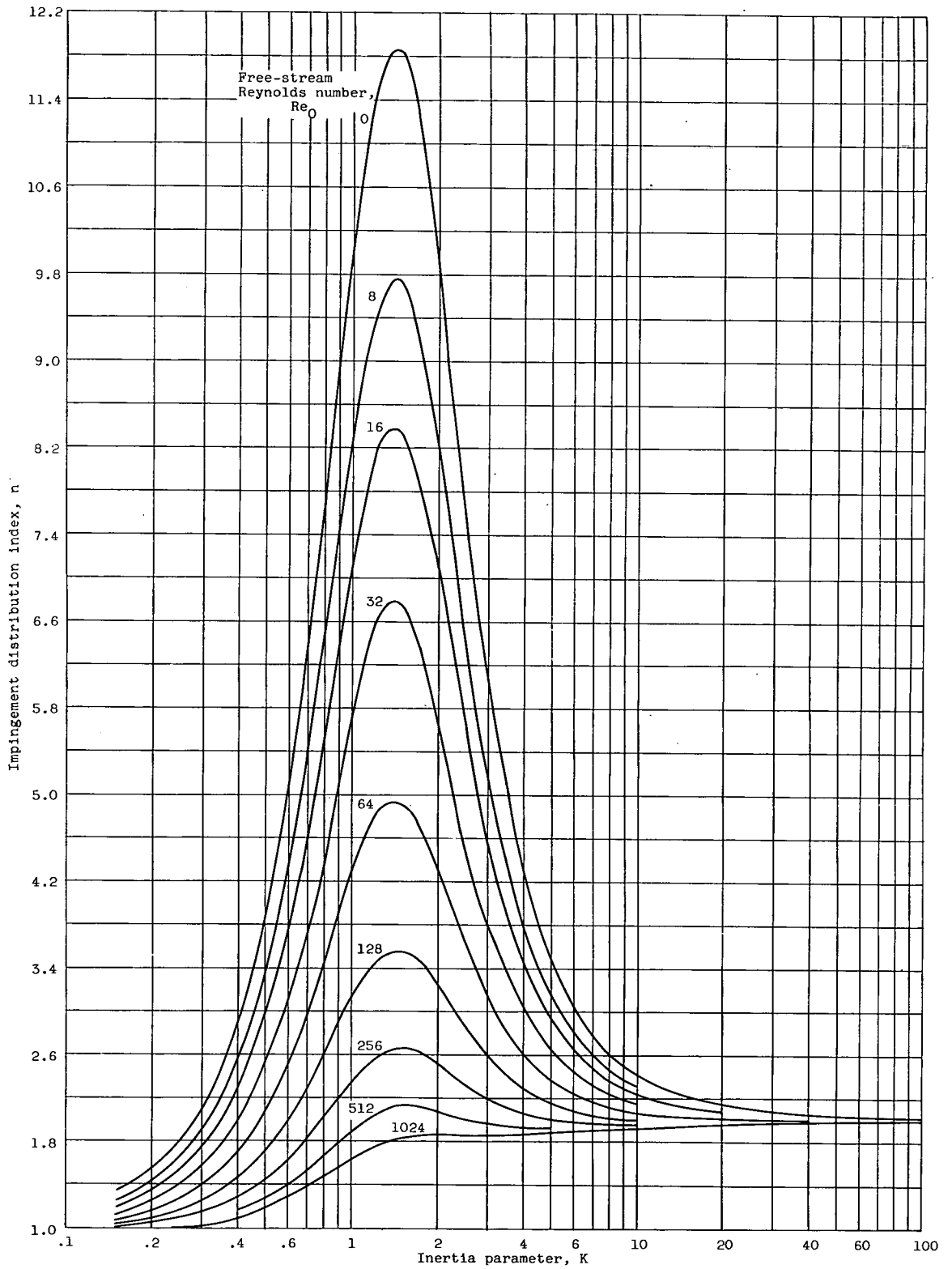


Figure 3. - Impingement distribution index calculated from equation (19).

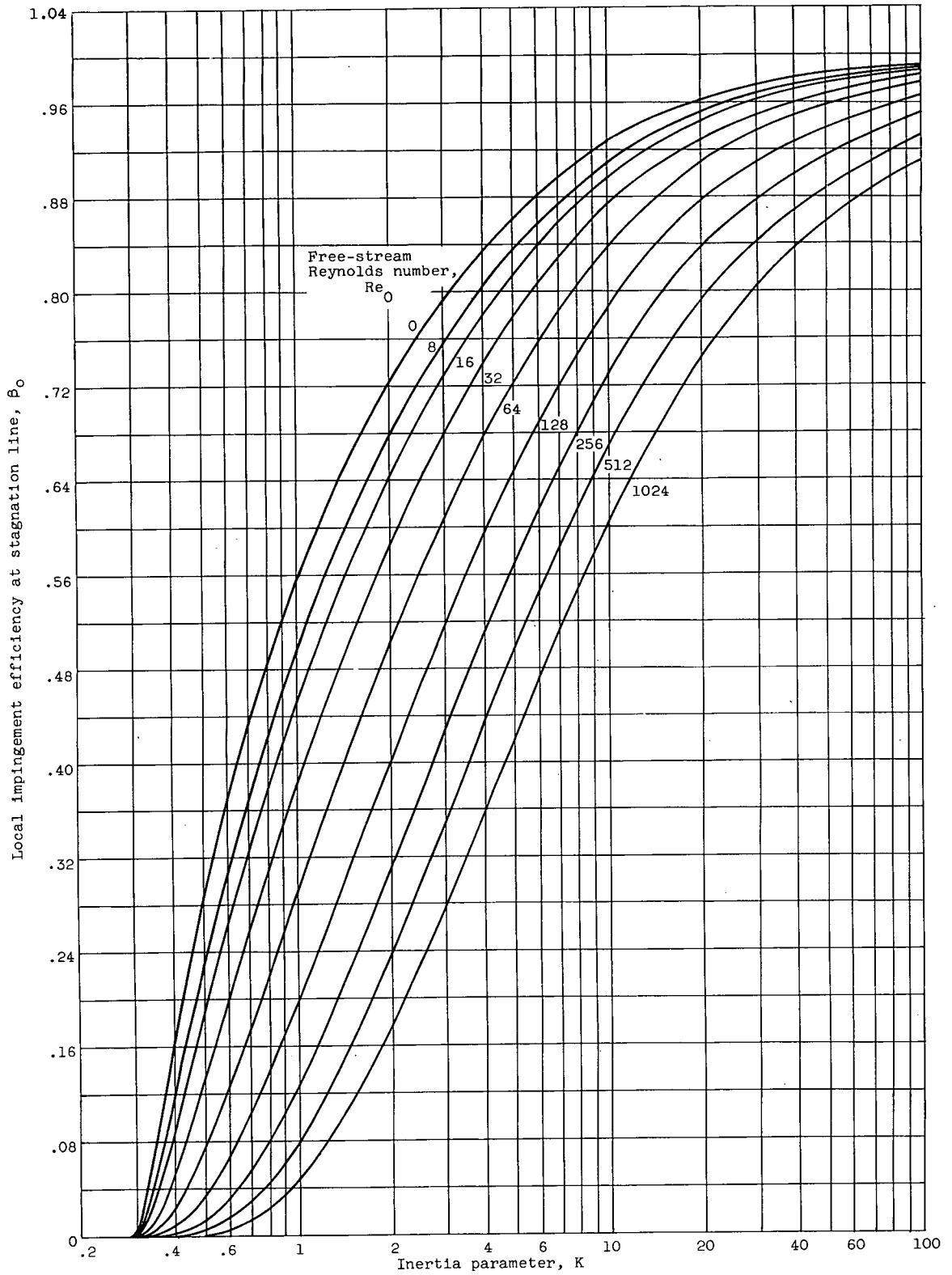


Figure 4. - Local impingement efficiency at stagnation line calculated from equation (20).

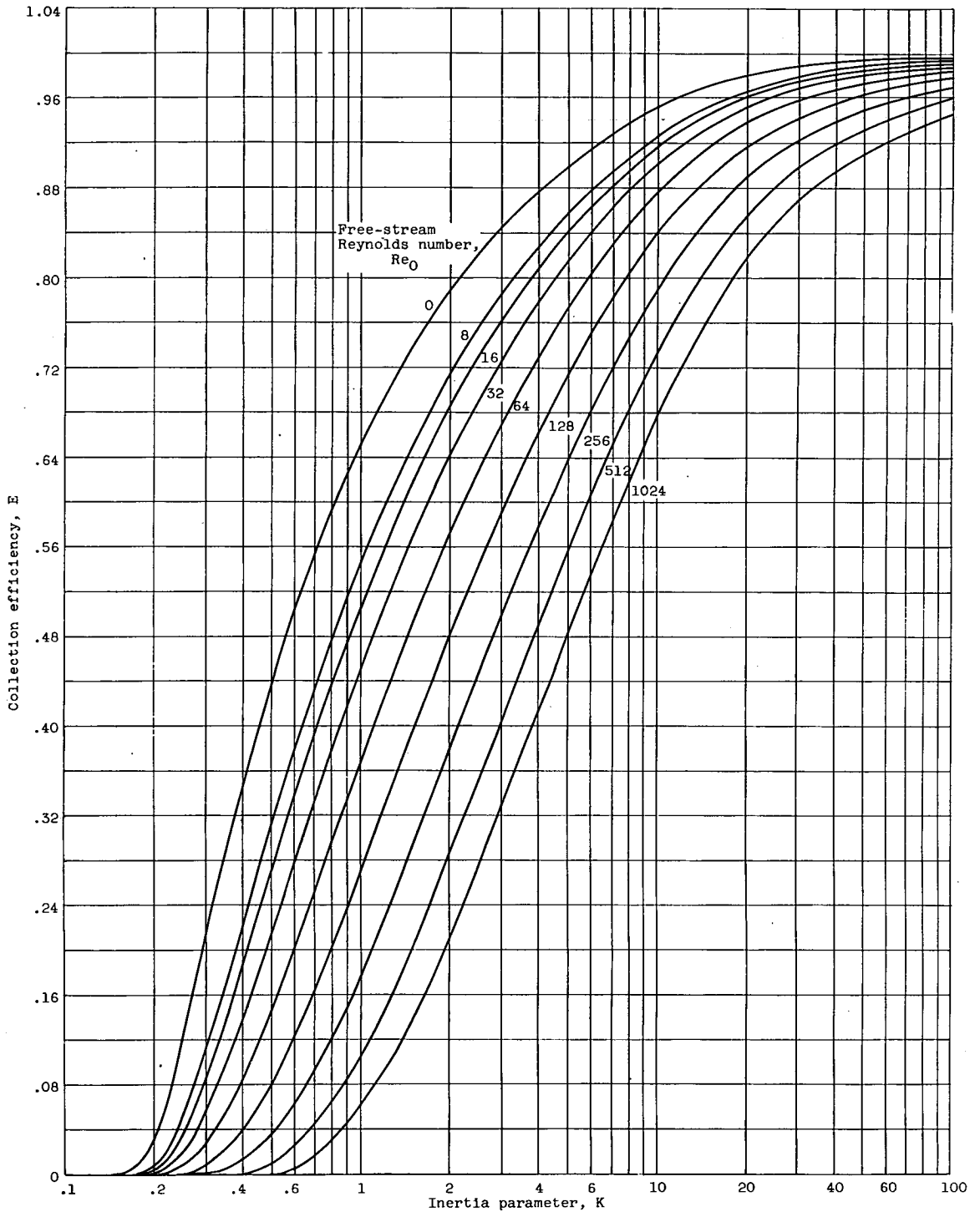


Figure 5. - Collection efficiency calculated from equation (21).

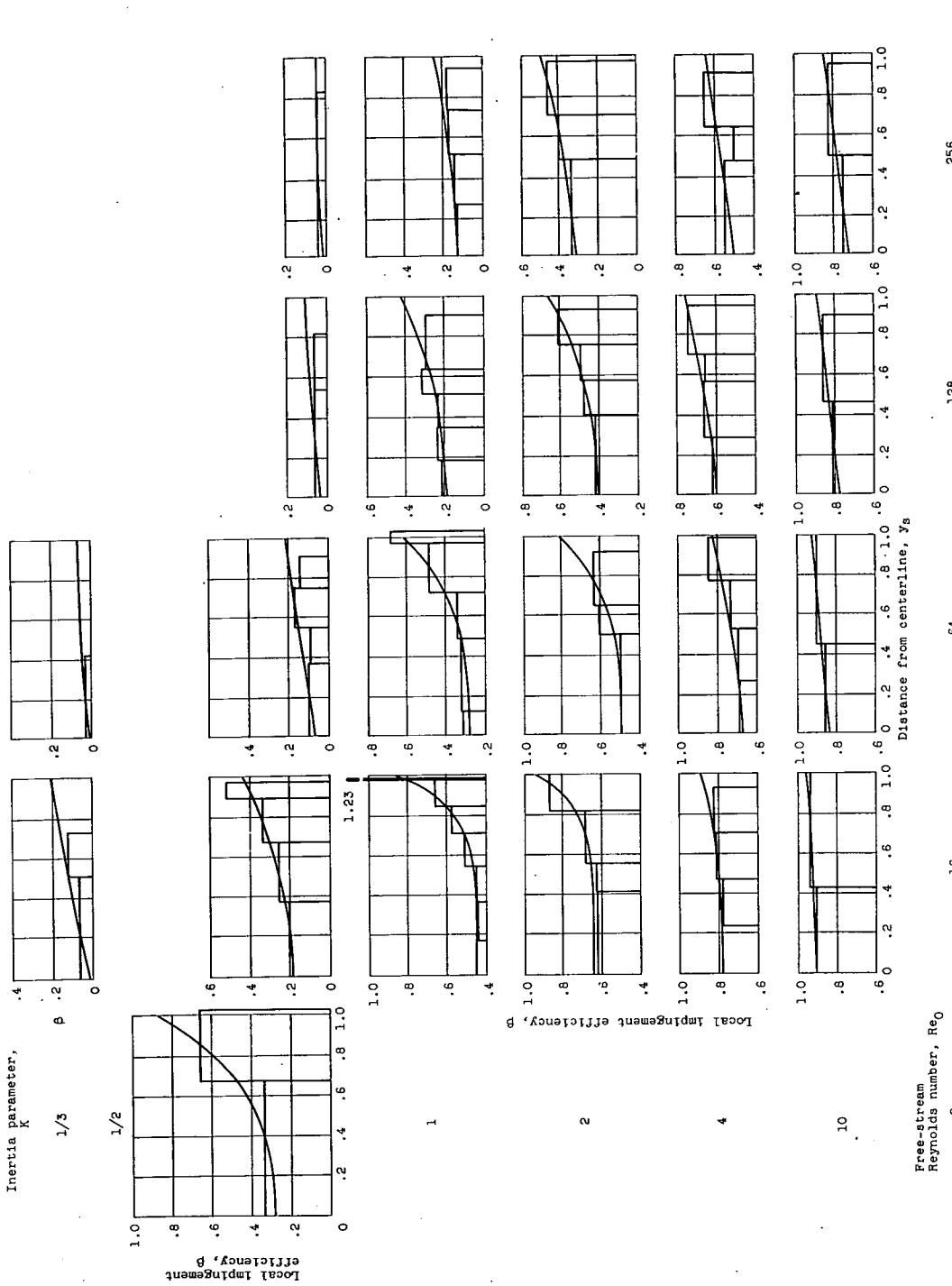


Figure 6. - Comparison of impingement profiles showing local impingement efficiency as function of dimensionless distance from centerline for various combinations of  $k$  and  $Re_0$ . (Curves calculated from eq. (17) using values of  $n$ ,  $\beta_0$ , and  $E$  from eqs. (19), (20), and (21). Block diagrams show average values from eq. (22) for intervals between individual trajectories calculated with differential analyzer.)